RESEARCH ARTICLE
SPACE PHYSICS: MAGNETOSPHERIC PHYSICS

Earth and Planetary Physics
8: 375–381, 2024
doi: 10.26464/epp2024015

Extreme value theory applied to the auroral electrojet indices

Si Chen[1], Hong Yuan[1*], Yong Wei[2,3], Guang Yang[1], and FengZheng Yu[1]

[1]Aerospace Information Research Institute, Chinese Academy of Sciences, Beijing 100094, China;

[2]Key Laboratory of Earth and Planetary Physics, Institute of Geology and Geophysics, Chinese Academy of Sciences, Beijing 100029, China;

[3]College of Earth and Planetary Sciences, University of Chinese Academy of Sciences, Beijing 100049, China

Key Points:

- By fitting the generalized Pareto distribution to the auroral electrojet (*AE*) index, negative shape parameters were obtained, suggesting the existence of an upper limit to the *AE* index.
- Understanding the plateau of *AE* values is crucial for assessing the risks associated with extreme events.
- Although values surpassing the upper limit are rare, their existence underscores the need for diligent precautions to mitigate the consequences of such extreme events and for careful consideration in planning and preparedness efforts.

Citation: Chen, S., Yuan, H., Wei, Y., Yang, G., and Yu, F. Z. (2024). Extreme value theory applied to the auroral electrojet indices. *Earth Planet. Phys.*, *8*(2), 375–381. http://doi.org/10.26464/epp2024015

Abstract: The study of extreme weather and space events has gained paramount importance in modern society owing to rapid advances in high technology. Understanding and describing exceptional occurrences plays a crucial role in making decisive assessments of their potential impact on technical, economic, and social aspects in various fields. This research focuses on analyzing the hourly values of the auroral electrojet (*AE*) geomagnetic index from 1957 to 2019 by using the peak over threshold method in extreme value theory. By fitting the generalized Pareto distribution to extreme *AE* values, shape parameter indices were derived, revealing negative values that establish an upper bound for this time series. Consequently, it became evident that the *AE* values had reached a plateau, suggesting that extreme events exceeding the established upper limit are rare. As a result, although the need for diligent precautions to mitigate the consequences of such extreme events persists, surpassing the upper limit of *AE* values becomes increasingly challenging. It is also possible to observe an aurora in the middle- and low-latitude regions during the maximum period of the *AE* index.

Keywords: auroral electrojet indices; extreme value theory; extreme events

1. Introduction

Throughout the course of history, human fascination with auroras has persisted, as evidenced by the presence of observational records in historical texts from East Asia and Europe (Krivský and Pejml, 1988; Lee et al., 2004; Wang YQ et al., 2021). These luminous displays not only captivate our senses but also offer valuable insights into the physical processes of energy transfer and transformation within the space environment. However, the magnificence of auroras corresponds to the intensity of associated geomagnetic storms (Piddington, 1964; Yokoyama et al., 1998; He F et al., 2023). These storms can trigger profound disturbances in the Earth's magnetosphere and ionosphere, and severe occurrences have resulted in global magnetic disruptions (Gonzalez et al., 1994; Fu HS et al., 2011; Chen YQ et al., 2023). The multifaceted consequences of geomagnetic storms encompass disruptions to ground communication and satellite operations. Of particular interest is the impact on particle motion in the upper atmosphere during these storms, which results in increased aerodynamic drag on spacecraft navigating through space (Bruinsma et al., 2021; Dang T et al., 2022; Berger et al., 2023). Geomagnetic storms predominantly affect near-Earth orbits situated below nearly 500 km and inject a substantial amount of energy into the polar regions (Li X et al., 2013; Huang FQ et al., 2021). This energy propagates to the upper atmosphere, inducing atmospheric heating and extending to lower latitude regions. Consequently, the lower atmosphere undergoes heating, expansion, and increased gas density in satellite orbits, resulting in augmented drag on satellites. As a result, satellites experience decreased speed and altitude, which poses challenges to maintaining their designated orbital height (Li RX and Lei JH, 2021; Li RX et al., 2023). Thus, to ensure the proper functioning of low-Earth-orbit satellites, artificial boosting back to their original orbital height is required when they descend to a specific position. Consequently, the strength of geomagnetic storms directly correlates to the level of threat posed to ground communication and satellite operations. The auroral electrojet (*AE*) index serves as a globally quantifiable measurement that represents the current flow of auroral-induced geomagnetic disturbances below and within the auroral oval (Frey, 2007; Edemskiy and Yasyukevich, 2022). Additionally, the *AE* index, introduced by Davis and Sugiura (1966), correlates with the

First author: S. Chen, chensi@aircas.ac.cn
Correspondence to: Yuan H., yuanhong@aircas.ac.cn
Received 22 NOV 2023; Accepted 31 JAN 2024.
First Published online 27 FEB 2024.

physical processes of energy release in the magnetotail resulting from the interaction between the solar wind and the magnetosphere (Kauristie et al., 2017). Calculated from the horizontal-component data of seven auroral stations over a 6-d period, the *AE* index can effectively represent the total auroral current (Davis and Sugiura, 1966; Kauristie et al., 2017). Extreme *AE* indices signify heightened auroral activity, leading to auroral substorms, which can be identified by observing peak values of the *AE* index. Such extreme *AE* events increase the probability of observing auroras in the low- and middle-latitude regions. Extreme aurora electrode activity causes severe disturbances in the geomagnetic field and ionosphere, changing rapidly and resulting in a huge geomagnetic-induced current (GIC). The GIC can affect and damage power grids and pipelines; thus, the impact of the auroral latitude on the GIC has begun attracting attention (Beggan, 2015). Such disturbances also have adverse effects on communication systems and satellite systems. Understanding the fluctuations in these indices is critical to adequately preparing for future large-scale solar eruptions and potential damage to infrastructure, as well as the possibility of observing auroras in the low- and middle-latitude regions.

This work utilizes extreme value theory (EVT) as a method to estimate the probability of extreme *AE* events occurring. Extreme value theory was selected because of its ability to account for the higher probability of the occurrence of an extreme event compared with Gaussian distribution estimations, which exhibit a "heavy tail" phenomenon (Gumbel, 1958; Coles, 2001). Extreme value theory is particularly suitable for analyzing time series data with nonstationary characteristics, and it enables estimation of the probability of extreme events (Coles, 2001). Extreme value theory has been extensively used in space physics research, as demonstrated by previous studies. For instance, Ramos (2007) applied EVT to analyze sunspot numbers to obtain the statistical properties of solar cycle extremes. Acero et al. (2017, 2018, 2019) also applied EVT to analyze sunspot numbers, as well as the disturbance storm-time (*Dst*) index and the daily solar radio flux at 10.7 cm. They found that the data had a upper limit, and they estimated the return levels. Chen S et al. (2019, 2021) applied EVT to the geomagnetic *Aa* index (which can describe the quantitatively of magnetic activity) and ancient auroral records to estimate the probability of extreme geomagnetic storms, and they connected the auroral records with space events.

In this work, the peak over threshold (POT) method in EVT was chosen. The POT method is mainly used to analyze extreme data above a certain threshold, which can avoid the waste of data, especially when the extreme data are sparse (Coles, 2001). More extreme data could give more accurate estimations and be more robust (Coles, 2001; Chen S et al., 2019). The POT was applied to study the completed *AE* index up to the present. The primary objectives were to estimate the probability of occurrence of extreme *AE* events and to assess the likelihood of aurora events. By examining historical information on auroras, scientists can establish long-term patterns of space weather variability and solar activity spanning from decades to millennia (Usoskin, 2017; Riley et al., 2018; Mandea and Chambodut, 2020). This information is crucial for anticipating potential large-scale solar eruptions and implementing measures to minimize the potential infrastructure damage linked to such occurrences.

2. Materials and Methods

The *AE* index was provided by the World Data Center for Geomagnetism located at Kyoto University in Japan (https://wdc.kugi.kyoto-u.ac.jp/aeasy/index.html). The *AE* index was proposed by Davis and Sugiura (1966) to characterize the global auroral current. Auroral electrojet indices are derived from geomagnetic variations in the horizontal component observed at 10–13 selected observatories along the auroral region in the Northern Hemisphere. A base value for each monthly station was first calculated by averaging all data for the station on the five quietest days internationally to normalize the data. This base value was subtracted from each value of 1 min of data obtained at the station during the month. The maximum and minimum values were then selected among the data from all stations at each given time (universal time). In this study, we used the hourly *AE* index. The more observatories used, the more reliable is the *AE* index. However, the distribution of observatories along the aurora is not uniform. The distribution of *AE* sites is shown in Table 1. Figure 1 shows the time series of the *AE* index in this study from 1957 to 2019.

Extreme value theory is one if the statistical methods used for extreme events. When the sample size is large, the probability of extreme values being distributed at the tail is more significant (Coles, 2001). The POT method models the data over a selected threshold to a generalized Pareto distribution (GPD). The distribution is approximated as (Coles, 2001)

$$P\{X-u<y|X>u\}=1-\left(1+\frac{\xi y}{\sigma}y\right)^{-1/\xi}, \tag{1}$$

where u is the threshold, σ is the scale parameter, ξ is the shape parameter, the scale parameter is about the GPD, and the shape parameter is about the tail information of the GPD. The parameters in the GPD were calculated by the maximum likelihood estimation (MLE), and the confidence intervals (CIs) were calculated by the bootstrapping procedure (Gilleland and Katz, 2016).

To effectively analyze the hourly *AE* index and determine the probability of *AE* activities, it is crucial to define a suitable threshold u. Setting the threshold too low will result in the model estimation deviating from the asymptotic basis. This can occur when too few samples of extreme events are available, leading to high variance (Coles, 2001). Conversely, setting the threshold too high may also introduce issues with high variance (Coles, 2001). Coles (2001) emphasized the importance of finding parameter estimate stability and proposed a method for selecting the best threshold. To ensure parameter estimate stability, it is recommended to plot the parameters with the mean excess plot and threshold plots, specifically the scale parameter σ and shape parameter ξ, against different values of the threshold u (Coles, 2001). By examining these plots, one can observe whether the parameter estimates remain stable within their sampling errors. It should be noted that although these estimates may not be exactly constant, they should exhibit stability within a certain range of the threshold (Coles, 2001). The extreme events that EVT requires for analysis

Table 1. Distribution of the *AE* stations.

Observatory	Geographic coordinates		Geomagnetic coordinates	
	Latitude (°N)	Longitude (°E)	Latitude (°N)	Longitude (°E)
Abisko	68.36	18.82	66.04	115.08
Dixon Island	73.55	80.57	63.02	161.57
Cape Chelyuskin	77.72	104.28	66.26	176.46
Tixie Bay	71.58	129	60.44	191.41
Cape Wellen	66.17	190.17	61.79	237.1
Barrow	71.3	203.25	68.54	241.15
College	64.87	212.17	64.63	256.52
Yellowknife	62.4	245.6	69	292.8
Fort Churchill	58.8	265.9	68.7	322.77
Poste-de-la-Baleine	55.27	282.22	66.58	347.36
Narsarsuaq (Narssarssuaq)	61.2	314.16	71.21	36.79
Leirvogur	64.18	338.3	70.22	71.04

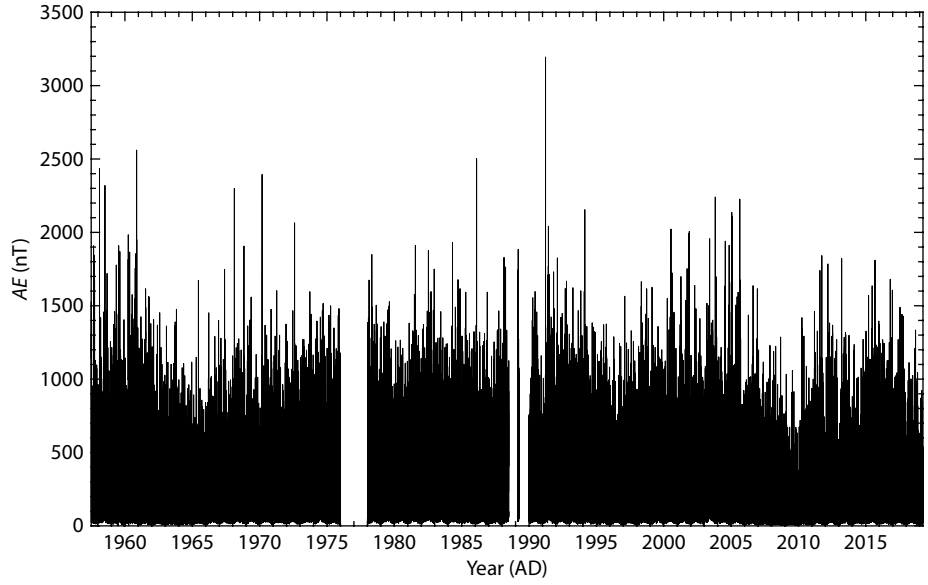

Figure 1. Time series of the hourly *AE* index from 1957 to 2019.

are independent (Coles, 2001). Considering the timing of magnetic storms and auroral substorms, the geomagnetic index will generally last for 3 d and the geomagnetic index will be very high (Chen S et al., 2019). We determined the maximum value of the *AE* index for three consecutive days as the same extreme event. Therefore, the extreme *AE* events were obtained with the declustering process with the running length (determined *r*) of r = 3 d before applying the EVT analysis to the data.

According to Coles (2001), in EVT, if the shape parameter $\xi < 0$, the distribution has an upper bound, which can be represented as $u - \sigma/\xi$. In this study, we estimated the parameters and calculated the CIs for all fitting parameters and return levels by using the bootstrap procedure (Gilleland and Katz, 2016). We used the POT method to analyze the hourly *AE* index. The results obtained using this method provided valuable insights into the probability of occurrence of *AE* events.

3. Results

In this study, the *AE* index above the thresholds from 1957 to 2019 was analyzed by using the GPD model. We analyzed the data from the extreme tail part, that is, the highest *AE* index. To apply the GPD to the *AE* index, it is vital to define a suitable threshold u. The model estimation will deviate from the asymptotic basis when u is too low; the samples of extreme events may be too few and cause high variance when u is too high (Coles, 2001). As shown by Coles (2001), it is necessary to find the parameter estimate stability.

Here, we used mean excess plots and parameter estimates to assess the reliability of the fitted GPD model (Coles, 2001). The mean excess, which represents the average of observations above the threshold u, is a key factor in evaluating the proximity of these observations to the GPD model. A nearly constant mean excess suggests that observations above the threshold closely align with the GPD model, indicating a more reliable fit (Coles, 2001).

Figure 2a illustrates the mean excess plot for the *AE* index, showing the relationship between the threshold u and the average excess value. We observed that when the threshold u exceeded 1460 nT, the CIs became large. This result indicated that the observations above this threshold closely adhered to the GPD model. Generally, an average excess plot provides a range of suitable thresholds. However, in practice, selecting the thresholds solely based on the average remaining life can be challenging, thus highlighting the importance of examining the parameter estimate stability (Coles, 2001). To determine the stability of the parameter estimates, we focused on the scale parameter σ and the shape parameter ξ, both of which should exhibit stability with respect to the threshold u, and their CIs should be narrow. Although the sampling variability suggests that these estimates may not be perfectly constant, they should demonstrate stability within the range of the sampling error (Coles, 2001). Figure 2b presents the parameter estimate plot, particularly highlighting the stability of the shape parameter ξ within the threshold range above 1460 nT. Notably, the shape parameter remains stable, indicating that the underlying distribution possesses consistent upper tail behavior. Moreover, the CIs (represented by vertical lines) for both the scale and shape parameters are relatively small. These findings further support the stability and reliability of the parameter estimates. In summary, our analysis demonstrates that the GPD model provides a reliable fit for the *AE* index data. The mean excess values indicate consistent adherence to the GPD model above the threshold of 1460 nT. Furthermore, the stability of the parameter estimates, particularly the shape parameter, and the small CIs reinforce the validity of the fitted model. As depicted in Figure 2, the parameters exhibited variation at different thresholds. Notably, when u exceeded 1460 nT, the CIs expanded, and the parameters of σ and ξ became unstable. Therefore, we selected a threshold value of 1460 nT, obtaining 128 extreme values. The parameters of the GPD model applied to the *AE* index were obtained by the MLE method (Gilleland and Katz, 2016), the ξ [95% CIs] = −0.01 [−0.18, 0.16], and the σ [95% CIs] = 278.15 [211.49, 344.81].

To further assess the fit of the GPD model, we assessed plots for the fit of the POT method to the *AE* index over the threshold of u =1460 nT. The probability plot of the GPD is shown in Figure 3a. As shown in Figure 3a, the plot could intuitively reflect the situation of reasonable GPD fitting. All points comprising the model fitting probability and the empirical probability are close to linear. Figure 3b is a plot of randomly generated data from the GPD fitting against the empirical data quantiles, which are also nearly linear. As shown in Figure 3c, the density estimate plot seems consistent with the empirical plot and the histogram of the data. Figure 3 mainly shows that the fitted GPD model was valid for the *AE* analyzed.

Figure 4 shows the return level when estimating the *AE* index by using the GPD model. As the return period increases, the *AE* index also increases, and the data will reach a plateau as the return period increases. This result also implies that the *AE* index has an upper bound, which is consistent with the negative shape parameter obtained. Through Figure 4, we can estimate the return level corresponding to different return periods. For example, we can estimate the *AE* estimate corresponding to any time. We used this

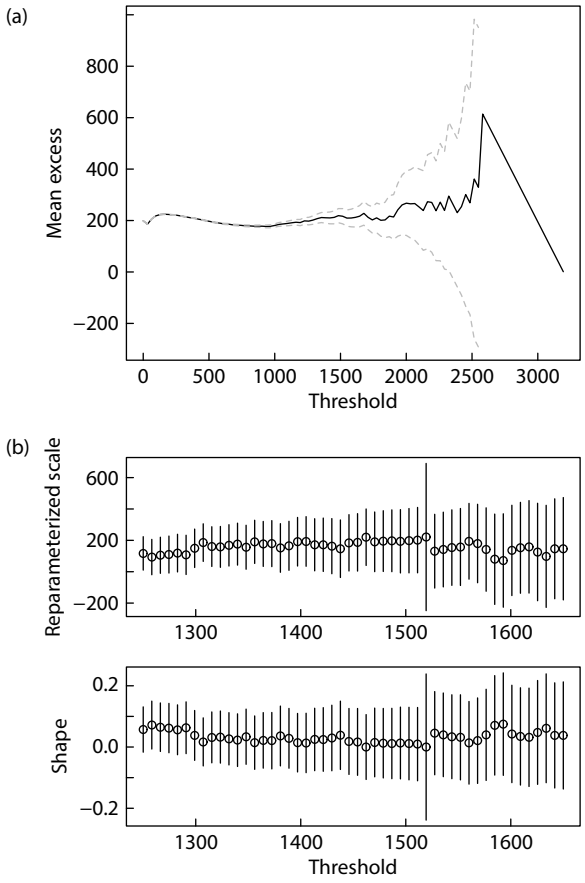

Figure 2. (a) Plot of the mean residual life of the *AE* index. The dashed line is the 95% CI. (b) Parameter estimates for the *AE* index thresholds. The vertical lines represent 95% CIs.

method to estimate the return level of the *AE* index with 11-, 22-, 50-, 100-, 200-, and 550-year return periods. As shown in Table 2, the 100-year return level is 2917.267 [2441.845, 3392.690], and the 200-year return level is 3098.633 [2484.574, 3712.692]. These observations hold significance for predicting the likelihood of future events, wherein the use of EVT allows for the estimation of return levels and return periods.

4. Discussion and Conclusions

Previous studies have also investigated *AE* activities (Thomson et al., 2011; Nakamura et al., 2015). However, Thomson et al. (2011) studied horizontal magnetic field variations in the auroral latitude, which increased with the return period and had no upper limit. In contrast, Nakamura et al. (2015) pointed out an upper limit to changes in the geomagnetic *AU* and *AL* indices, but no upper limit for the *AE* index. Maybe because of data limitations or other unknown reasons, research still needs to move forward based on previous research. In addition, the reasonable selection of parameters for the correct use of the POT and more data provide strong support for drawing more reasonable conclusions. This work investigates the *AE* index by applying EVT to the *AE* index (1957–2019) for hourly scales. For this, we used the POT method, which considers all *AE* indices exceeding a predefined upper threshold u after declustering, which could be modeled by using the GPD. According to the findings, the diagnostic plot of extreme

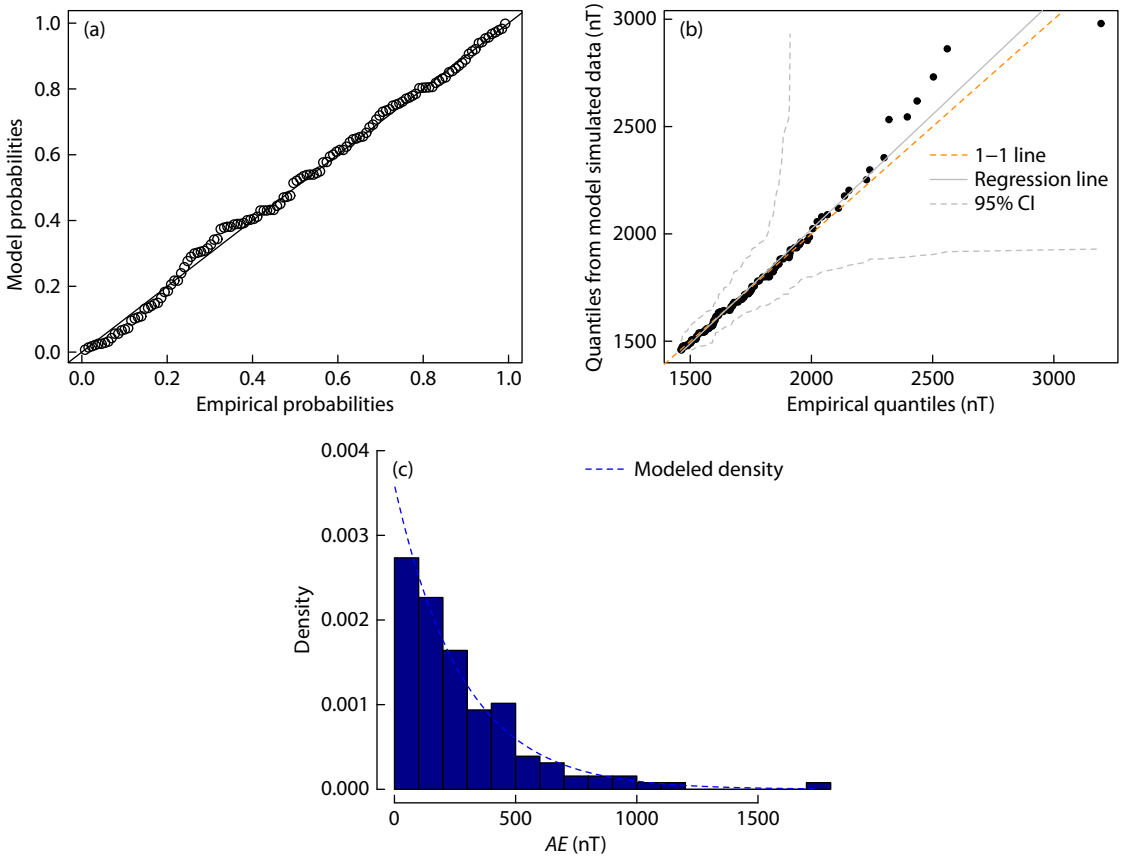

Figure 3. Plots assessed for the fit of the POT method to the *AE* index from 1957 to 2019. (a) The probability plot of the GPD model. The black points are the *AE* index, and the black line is the 1–1 line. (b) The quantile-quantile (QQ) plot with empirical quantile and model quantile simulated data. The solid gray line is the linear fit of the QQ plot, the dashed gray curves represent the 95% CI, the black dots are the observed *AE* index, and the dashed orange line is the 1–1 line. (c) Plot of the empirical density of the *AE* (histogram) with the GPD fit density (dashed blue line).

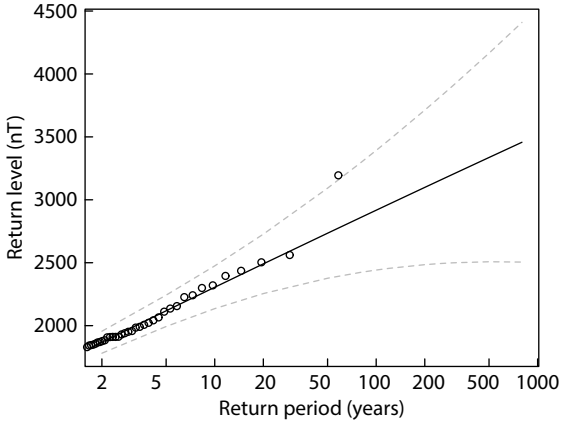

Figure 4. Return levels of the *AE* index with their return periods.

value results confirmed that the EVT model fit on hourly scales. The shape parameter obtained by this method was negative, which indicates that the data distribution had an upper bound. The obtained return levels on an hourly scale were 2516.399, 2734.557, 2917.267, and 3360.932 for N = 22, 50, 100, and 550 years. Of course, we must interpret these results with caution, especially over hundreds of years, because the estimated time of the return level is longer than the observed time.

In the POT approach, obtaining the optimal threshold u to study the extremes of the hourly *AE* index involves (1) considering the mean residual life plots, and (2) considering the parameters of the hourly *AE* with different threshold estimates. To identify independent clusters of extreme observations, we chose a length equal to r = 3 d because this value is approximately the time of magnetic storm occurrence (Acero et al., 2018; Chen S et al., 2019). For each cluster, we chose the date with the largest *AE*. When this technique was used, even considering the 95% CI (i.e., the extreme *AE* distribution), the shape parameter was negative, giving an upper bound. The amount of energy from the Sun that can be transmitted to the Earth through the solar wind has an upper limit. In this example, for N = 100, 200, and 550 years, the return levels obtained were 2917.267, 3098.633, and 3360.932, respectively. Through this method, we could estimate the return level of the *AE*

Table 2. Return levels of the *AE* index.

Return period (years)	Return level [95% CI]
11	2330.718 [2153.089, 2508.347]
22	2516.399 [2269.483, 2763.314]
50	2734.557 [2376.675, 3092.440]
100	2917.267 [2441.845, 3392.690]
200	3098.633 [2484.574, 3712.692]
550	3360.932 [2507.940, 4213.924]

index corresponding to any return period. This allowed us to estimate the probability of occurrence of AEs of different levels.

We applied the EVT method to the *AE* index, which allowed us to estimate the probability of occurrence of geomagnetic storms and auroral substorms. It may also provide relevant insights for auroral observations and geomagnetic storm monitoring. During the magnetic storm event on April 24, 2023, a red aurora was observed in the Karamay region of Xinjiang, China (geographical latitude of ~45.6°N), and in the World Data Center for Geomagnetism, the *AE* index showed that it exceeded 2000 nT. The Sun produces energy bursts and usually coronal holes in the atmosphere on the surface of the Sun, and the high-speed solar wind is largely abolished in areas with low coronal density. The coronal mass ejection is a form of solar eruption (Bravo et al., 1998), and information on the history of auroras can help scientists build long-term patterns of space weather variability and solar activity on timescales ranging from decades to millennia (Chen S et al., 2021; He F et al., 2021; Wang YQ et al., 2021). Understanding these fluctuations could help prepare for future massive solar eruptions and possible infrastructure damage (Lockwood et al., 2016, 2021).

Acknowledgments

The *AE* index was obtained from the World Data Center for Geomagnetism, Kyoto (https://wdc.kugi.kyoto-u.ac.jp/aeasy/index.html). The extRemes package in R software is available at the R Project for Statistical Computing.

References

Acero, F. J., Carrasco, V. M. S., Gallego, M. C., García, J. A., and Vaquero, J. M. (2017). Extreme value theory and the new sunspot number series. *Astrophys. J.*, *839*(2), 98. https://doi.org/10.3847/1538-4357/aa69bc

Acero, F. J., Vaquero, J. M., Gallego, M. C., and García, J. A. (2018). A limit for the values of the *Dst* geomagnetic index. *Geophys. Res. Lett.*, *45*(18), 9435–9440. https://doi.org/10.1029/2018GL079676

Acero, F. J., Vaquero, J. M., Gallego, M. C., and García, J. A. (2019). Extreme value theory applied to the daily solar radio flux at 10.7 cm. *Sol. Phys.*, *294*(6), 67. https://doi.org/10.1007/s11207-019-1457-z

Beggan, C. D. (2015). Sensitivity of geomagnetically induced currents to varying auroral electrojet and conductivity models. *Earth Planets Space*, *67*(1), 24. https://doi.org/10.1186/s40623-014-0168-9

Berger, T. E., Dominique, M., Lucas, G., Pilinski, M., Ray, V., Sewell, R., Sutton, E. K., Thayer, J. P., and Thiemann, E. (2023). The thermosphere is a drag: The 2022 Starlink incident and the threat of geomagnetic storms to low earth orbit space operations. *Space Wea.*, *21*(3), e2022SW003330. https://doi.org/10.1029/2022SW003330

Bravo, S., Cruz-Abeyro, J. A. L., and Rojas, D. (1998). The spatial relationship between active regions and coronal holes and the occurrence of intense geomagnetic storms throughout the solar activity cycle. *Ann. Geophys.*, *16*(1), 49–54. https://doi.org/10.1007/s00585-997-0049-7

Bruinsma, S., Boniface, C., Sutton, E. K., and Fedrizzi, M. (2021). Thermosphere modeling capabilities assessment: Geomagnetic storms. *J. Space Wea. Space Climate*, *11*, 12. https://doi.org/10.1051/swsc/2021002

Chen, S., Chai, L. H., Xu, K. H., Wei, Y., Rong, Z. J., and Wan, W. X. (2019). Estimation of the occurrence probability of extreme geomagnetic storms by applying extreme value theory to Aa index. *J. Geophys. Res.: Space Phys.*, *124*(12), 9943–9952. https://doi.org/10.1029/2019JA026947

Chen, S., Wei, Y., He, F., Yue, X. N., Xu, K. H., Wang, Y. Q., Chai, L. H., and Yan, L. M. (2021). Evaluation of the 900 - year European auroral records with extreme value theory. *J. Geophys. Res.: Space Phys.*, *126*(11), e2021JA029481. https://doi.org/10.1029/2021ja029481

Chen, Y. Q., Wu, M. Y., Chen, Y. J., Xiao, S. D., Wang, G. Q., and Zhang, T. L. (2023). Responses of the field-aligned currents in the plasma sheet boundary layer to a geomagnetic storm. *Earth Planet. Phys.*, *7*(5), 558–564. https://doi.org/10.26464/epp2023075

Coles, S. (2001). *An Introduction to Statistical Modeling of Extreme Values*. London: Springer. https://doi.org/10.1007/978-1-4471-3675-0

Dang, T., Li, X. L., Luo, B. X., Li, R. X., Zhang, B. Z., Pham, K., Ren, D. X., Chen, X. T., Lei, J. H., and Wang, Y. M. (2022). Unveiling the space weather during the Starlink satellites destruction event on 4 February 2022. *Space Wea.*, *20*(8), e2022SW003152. https://doi.org/10.1029/2022SW003152

Davis, T. N., and Sugiura, M. (1966). Auroral electrojet activity index *AE* and its universal time variations. *J. Geophys. Res.*, *71*(3), 785–801. https://doi.org/10.1029/JZ071i003p00785

Edemskiy, I. K., and Yasyukevich, Y. V. (2022). Auroral oval boundary dynamics on the nature of geomagnetic storm. *Remote Sens.*, *14*(21), 5486. https://doi.org/10.3390/rs14215486

Frey, H. U. (2007). Localized aurora beyond the auroral oval. *Rev. Geophys.*, *45*(1), RG1003. https://doi.org/10.1029/2005RG000174

Fu, H. S., Cao, J. B., Yang, B., and Lu, H. Y. (2011). Electron loss and acceleration during storm time: The contribution of wave–particle interaction, radial diffusion, and transport processes. *J. Geophys. Res.: Space Phys.*, *116*(A10), A10210. https://doi.org/10.1029/2011ja016672

Gilleland, E., and Katz, R. W. (2016). extRemes 2.0: An extreme value analysis package in R. *J. Stat. Softw.*, *72*(8), 1–39. https://doi.org/10.18637/jss.v072.i08

Gonzalez, W. D., Joselyn, J. A., Kamide, Y., Kroehl, H. W., Rostoker, G., Tsurutani, B. T., and Vasyliunas, V. M. (1994). What is a geomagnetic storm?. *J. Geophys. Res.: Space Phys.*, *99*(A4), 5771–5792. https://doi.org/10.1029/93ja02867

Gumbel, E. J. (1958). *Statistics of Extremes*. NewYork: Columbia University Press. https://doi.org/10.7312/gumb92958

He, F., Wei, Y., Maffei, S., Livermore, P. W., Davies, C. J., Mound, J., Xu, K. H., Cai, S. H., and Zhu, R. X. (2021). Equatorial auroral records reveal dynamics of the paleo-West Pacific geomagnetic anomaly. *Proc. Natl. Acad. Sci. US A*, *118*(20), e2026080118. https://doi.org/10.1073/pnas.2026080118

He, F., Yao, Z. H., Ni, B. B., Cao, X., Ye, S. Y., Guo, R. L., Li, J. X., Ren, Z. P., Yue, X. A., Zhang, Y. L., Wei, Y., Zhang, X. X., and Pu, Z. Y. (2023). Sawtooth and dune auroras simultaneously driven by waves around the plasmapause. *Earth Planet. Phys.*, *7*(2), 237–246. https://doi.org/10.26464/epp2023023

Huang, F. Q., Lei, J. H., Xiong, C., Zhong, J. H., and Li, G. Z. (2021). Observations of equatorial plasma bubbles during the geomagnetic storm of October 2016. *Earth Planet. Phys.*, *5*(5), 416–426. https://doi.org/10.26464/epp2021043

Kauristie, K., Morschhauser, A., Olsen, N., Finlay, C. C., McPherron, R. L., Gjerloev, J. W., and Opgenoorth, H. J. (2017). On the usage of geomagnetic indices for data selection in internal field modelling. *Space Sci. Rev.*, *206*(1-4), 61–90. https://doi.org/10.1007/s11214-016-0301-0

Krivský, L., and Pejml, K. (1988). *Solar Activity, Aurorae and Climate in Central Europe in the Last 1000 Years* (Vol. 75). Publications of the Astronomical Institute of the Czechoslovak Academy of Sciences.

Lee, E. H., Ahn, Y. S., Yang, H. J., and Chen, K. Y. (2004). The sunspot and auroral activity cycle derived from Korean historical records of the 11th–18th century. *Sol. Phys.*, *224*(1-2), 373–386. https://doi.org/10.1007/s11207-005-5199-8

Li, R. X., and Lei, J. H. (2021). The determination of satellite orbital decay from POD data during geomagnetic storms. *Space Wea.*, *19*(4), e2020SW002664. https://doi.org/10.1029/2020sw002664

Li, R. X., Lei, J. H., Kusche, J., Dang, T., Huang, F. Q., Luan, X. L., Zhang, S. R., Yan, M. D., Yang, Z. Y., ... Dou, X. (2023). Large-scale disturbances in the upper thermosphere induced by the 2022 Tonga volcanic eruption. *Geophys. Res. Lett.*, *50*(3), e2022GL102265. https://doi.org/10.1029/2022GL102265

Li, X., Schiller, Q., Blum, L., Califf, S., Zhao, H., Tu, W., Turner, D. L., Gerhardt, D., Palo, S., ... Spence, H. (2013). First results from CSSWE CubeSat: Characteristics of relativistic electrons in the near-Earth environment during the October 2012 magnetic storms. *J. Geophys. Res.: Space Phys.*, *118*(10), 6489–6499. https://doi.org/10.1002/2013JA019342

Lockwood, M., Owens, M., Barnard, L., Scott, C. J., Usoskin, I. G., Nevanlinna, H. (2016). Tests of sunspot number sequences: 2. Using geomagnetic and auroral data. *Sol. Phys.*, *291*(9-10), 2811–2828. https://doi.org/10.1007/s11207-016-0913-2

Lockwood, M., Haines, C., Barnard, L. A., Owens, M. J., Scott, C. J., Chambodut, A., and Mcwilliams, K. A. (2021). Semi-annual, annual and Universal Time variations in the magnetosphere and in geomagnetic activity: 4. Polar Cap motions and origins of the Universal Time effect. *J. Space Wea. Space Climate*, *11*, 15. https://doi.org/10.1051/swsc/2020077

Mandea, M., and Chambodut, A. (2020). Geomagnetic field processes and their implications for space weather. *Surv. Geophys.*, *41*(6), 1611–1627. https://doi.org/10.1007/s10712-020-09598-1

Nakamura, M., Yoneda, A., Oda, M., and Tsubouchi, K. (2015). Statistical analysis of extreme auroral electrojet indices. *Earth Planets Space*, *67*(1), 153. https://doi.org/10.1186/s40623-015-0321-0

Piddington, J. H. (1964). Geomagnetic storms, auroras and associated effects. *Space Sci. Rev.*, *3*(5), 724–780. https://doi.org/10.1007/BF00177956

Ramos, A. A. (2007). Extreme value theory and the solar cycle. *Astron. Astrophys.*, *472*(1), 293–298. https://doi.org/10.1051/0004-6361:20077574

Riley, P., Baker, D., Liu, Y. D., Verronen, P., Singer, H., and Güdel, M. (2018). Extreme space weather events: From cradle to grave. *Space Sci. Rev.*, *214*(1), 21. https://doi.org/10.1007/s11214-017-0456-3

Thomson, A. W. P., Dawson, E. B., and Reay, S. J. (2011). Quantifying extreme behavior in geomagnetic activity. *Space Wea.*, *9*(10), S10001. https://doi.org/10.1029/2011SW000696

Usoskin, I. G. (2017). A history of solar activity over millennia. *Liv. Rev. Sol. Phys.*, *14*(1), 3. https://doi.org/10.1007/s41116-017-0006-9

Wang, Y. Q., Chen, S., Xu, K. H., Yan, L. M., Yue, X. N., He, F., and Wei, Y. (2021). Ancient auroral records compiled from Korean historical books. *J. Geophys. Res.: Space Phys.*, *126*(1), e2020JA028763. https://doi.org/10.1029/2020JA028763

Yokoyama, N., Kamide, Y., and Miyaoka, H. (1998). The size of the auroral belt during magnetic storms. *Ann. Geophys.*, *16*(5), 566–573. https://doi.org/10.1007/s00585-998-0566-z